Microstructure-Mechanical Property Correlation in Size Controlled Nanocrystalline Molybdenum Films

*Anil K. Battu, Vishal B. Zade, Eva Deemer, and Chintalapalle V. Ramana**

The authors report on the microstructure, crystallography, and mechanical properties of size controlled nanocrystalline (nc) molybdenum (Mo) films deposited by sputtering. The nc-Mo films of ≈100 nm thick with a variable microstructure are deposited under variable argon (Ar) sputtering pressure (P_{Ar}), which is varied in the range of 3–25 mTorr. X-ray diffraction analyses indicate that the nc-Mo films exhibit (110) preferential growth. However, the crystal-quality degradation occurs for Mo films deposited at higher P_{Ar} due to difference in the adatom mobility. The average crystallite size (d) of the nc-Mo films is in the range of 5–20 nm; size decreases with increasing P_{Ar}. The effect of sputtering pressure is significant on the microstructure, which in turn influences the mechanical characteristics of Mo films. The hardness (H) and modulus of elasticity (E_r) of nc-Mo films deposited at lower P_{Ar} are higher but decreases continuously with increasing P_{Ar}. Under optimum sputtering conditions, the best mechanical characteristics obtained for Mo films are: $H = 25$ GPa, $E_r = 360$ GPa, $H/E_r = 0.07$, and $H^3/E_r^2 = 0.13$ GPa. A size-microstructure-mechanical property correlation in nc-Mo films is derived based on the results presented and discussed.

1. Introduction

Recent developments in surface coating technologies, particularly in the production of nanostructured films, have revealed exciting possibilities to control the structure and mechanical properties of thin films and surfaces. With combination of properties which were previously unattainable, the low dimensional nanostructured films provide unique opportunities for new directions in scientific research and technology development in diverse disciplines.[1,2] Current scientific thrust to produce the so-called "nanostructured and nanocomposite" coatings is directed primarily toward the design and development of super-hard or ultra-hard materials.[1–4] The performance and physical properties of these nanocrystalline materials are closely connected to their microstructure and are further controlled by defects, dislocations, grain boundaries, and interfaces.[1–6] For practical applications, materials' design phase must consider the combination of properties viz., hardness, elastic modulus, adhesion, toughness, and durability with low interfacial stresses.[4] For instance, the mechanical properties of metals are significantly modified when the grain size is reduced.[1,6,7] In nanostructured materials, the grain boundaries take up a relatively large volume-fraction of the system and can be expected to strongly influence their mechanical properties.[8] In fact, decreasing the average grain size in polycrystalline metals and alloys is the key approach to increase their mechanical strength.[9] Therefore, a fundamental understanding of the microstructure-mechanical property relationship in nanostructured materials is essential for utilizing them in complex functional device applications.

Exploring nanostructured metals, alloys, and metallic materials with better structural, chemical, and electrical properties has become a priority in view of the recent technological advancements and rapid industrialization. However, to accomplish the technological challenges, a fundamental understanding of the structure-mechanical property correlation in nanostructured metals and alloys is the key. Such a deeper understanding not only allows tuning the mechanical properties of metals and alloys for practical applications but also facilitates exploring new opportunities or applications. For instance, mechanical strength of polycrystalline metals and alloys can be significantly improved by controlling the average grain size. Smaller grain size contributes to the enhanced strength. The slip is arrested along the grain boundaries which further concocts a strengthening effect.[10] The Hall–Petch relationship is represented as[10,11]:

$$\sigma_y = \sigma_0 + kd^{-1/2} \quad (1)$$

where σ_0 is the friction stress resisting the motion of gliding dislocation, and k is the Hall–Petch slope, which is associated with a measure of the resistance of the grain boundary to slip transfer. For many decades, the classical Hall–Petch relationship has been successfully applied to explain the strength-size correlation in a wide variety of metals and alloys. However, it has to be pointed out that other phenomena such as relaxation processes at grain boundaries, associated with an extremely fine grain size, could lead to a decrease in strength and this could

Prof. C. V. Ramana, A. K. Battu, V. B. Zade
Department of Mechanical Engineering
University of Texas at El Paso
El Paso, Texas 79968, USA
E-mail: rvchintalapalle@utep.edu

Dr. E. Deemer
Department of Material Science and Engineering
University of Texas at El Paso
El Paso, Texas 79968, USA

DOI: 10.1002/adem.201800496

result in an inverse Hall–Petch relationship. Such inverse Hall–Petch relationship has been observed recently in Ta,[12] Cu,[13] Ni,[14] and Ni-W.[15]

The impetus for the present work was to derive a fundamental, scientific understanding of the structure-property correlation in molybdenum (Mo) films. With its inherent refractory property and high melting point, Molybdenum (Mo) presents itself as a viable material for a wide range of industrial applications.[16–24] A very high melting point of 2623 °C, low density ($\rho_{th} = 10.2\,g\,cm^{-3}$) and excellent strength-to-density ratio at high temperatures make Mo attractive for high-temperature applications.[18,19,22] The thermal expansion coefficient (a_{Mo}) of Mo is $5.75 \times 10^{-6}\ °C^{-1}$ at 1000 °C.[18] In addition, high creep, corrosion, and sputtering resistance makes Mo an interesting material for components used in aerospace and defense sector.[22] In addition, Mo finds quite interesting applications in solid lubrication,[25] where the lubricant material may be a powder or thin film, which reduces friction and wear of contacting surfaces in relative motion and provides protection from damage.[26] Molybdenum based compounds are specifically useful for extreme environment solid lubrication applications, such as space industry, where oils and greases must be avoided as they experience out gassing under high vacuum and high temperature conditions.[27] Mo has been extensively used owing to its excellent wear resistance as well. Mo further proves its usefulness in the field of electronics and optoelectronics with sputter-deposited films being widely used as a back-contact layer in CIS (copper indium selenide) and CIGS (copper indium gallium selenide) solar cells.[16] In case of the polycrystalline CIS/ CICS thin film solar cells, the metallic back contact serves as a substrate upon which the absorber layer is formed.[16,19,21] The excellent electrical properties coupled with mechanical durability during the absorber film growth has presides Mo over other competing metals as a choice for back contact.[16,19,21]

The physical, chemical, mechanical, and electronic properties of bulk and thin film Mo were ascertained by numerous investigations to test their viability for diverse technological applications. Most of the existing studies employed direct current (DC) magnetron sputtering for thin films. The resistivity and adhesion of Mo films vary as a function of working gas pressure.[28,29] Generally, higher sputtering gas pressure results in well adhesive but high resistivity Mo films, while lower pressure results in low resistivity but poor mechanical properties and adhesion.[16,19,21,28,29] Also, for DC sputter-deposited Mo films, a correlation is observed between the sputter gas pressure (P_{Ar}) and the stress within the deposited films.[17] Generally, Mo films deposited with low P_{Ar} were found to be under compressive stress, while those deposited with high pressures are found to be under tensile stress.[17] Recently, it has been demonstrated that the radio-frequency (RF) magnetron sputtering is an alternative key approach to deposit high quality Mo films for electronic and optoelectronic applications.[29–32] However, in some cases, adhesion properties of the Mo films were poor while desirable electrical properties can be obtained.[31] Thus, it is clear that there is a significant recent attention toward the structure and electronic property control of Mo films while maintaining good mechanical properties. However, while most of the earlier works were directed on relatively thicker coatings, efforts to understand the interplay between the growth, structure, and mechanical properties of thin Mo films (≤100 nm), where the substrate-film interface effects are dominant, are meager. In this context, the present work was performed on nanocrystalline Mo films deposited by RF magnetron sputtering at a relatively higher deposition temperature (200 °C). Efforts were made to understand the microstructure and mechanical characteristics of Mo films produced over a wide range of sputtering pressures. Compared to those reports exist on the relatively thicker Mo films in the literature, we paid utmost attention to the structural and mechanical properties of thin Mo films (≈100 nm), where the true effects of nanoscale dimensions and size are elucidated. It can be ascertained through our experimental findings that tuning processing conditions can provide a variable microstructure which has an influence on the mechanical properties. Experimental results further corroborate a size-structure-mechanical property correlation, which could be useful as a road-map print for Mo-based materials for a wide range of industrial applications.

2. Experimental Section

2.1. Fabrication

Nanocrystalline Mo films were deposited onto silicon (Si) (100) wafers by radio-frequency sputtering. The schematic layout of the sputtering system employed for the fabrication of Mo films is presented in **Figure 1**. The depostion procedures and details of the conditions employed are as follows. The Si(100) substrates were thoroughly cleaned by ultrasonication using ethyl alcohol and dried with nitrogen before introducing them into the vacuum chamber. The deposition chamber was evacuated to a base pressure of $\approx 10^{-7}$ Torr. A high purity (99.999%) Mo metal target (Plasmaterials, Inc.) of 2 in. diameter was employed to produce Mo films by sputtering the target with argon (Ar). The target to substrate distance was maintained at 7 cm, which was kept constant for all the Mo film depositions made. The sputtering power applied to the Mo target was slowly increased, while introducing high-purity Ar into the chamber to ignite the plasma. Upon sustained plasma conditions, target power was then slowly increased to 100 W, which was maintained constant during Mo film deposition. Before each deposition, the Mo target was pre-sputtered for 15 min with the sample shutter closed to obtain the stable plasma and remove the contaminants. Also, to ensure lateral isotropy of the Mo films, the Si(100) substrates were continuously rotated during the deposition at a rate of 3–4 rpm. A set of Mo films were deposited by varying the argon sputtering pressure (P_{Ar}) in the range of 3–25 mTorr while keeping the substrate temperature (T_s) constant at 200 °C. The Ar flow was controlled using MKS mass flow meters. The deposition was made to obtain a Mo film thickness of ≈100(±5) nm.

2.2. Characterization

2.2.1. Grazing Incidence X-Ray Diffraction (GIXRD)

The crystal structure analysis of the Mo films was performed using Grazing Incidence X-ray Diffraction (GIXRD). The

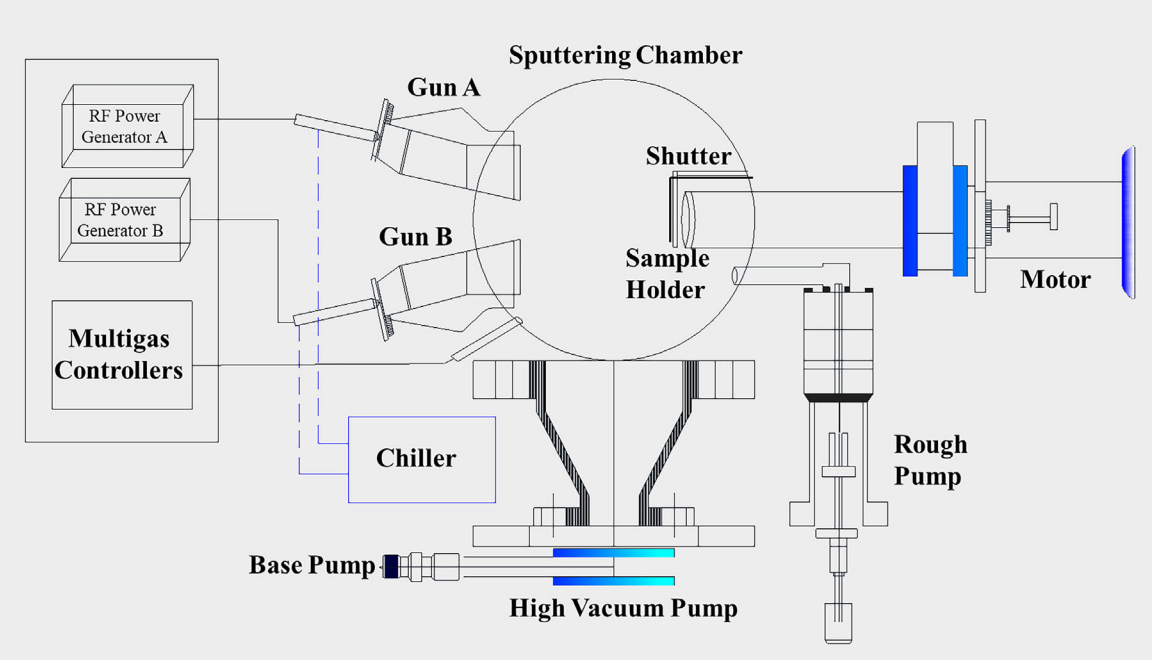

Figure 1. The schematic layout of the sputtering system employed for the fabrication of Mo films.

measurements were made at room temperature using a Bruker D8 advance, Cu-Kα radiation, and $\lambda = 1.54$ Å. All the measurements were made ex situ and as a function of variable P_{Ar}. In order to probe and study only surfaces and layers for the Mo films, the grazing incident angle was fixed to 1° for the incoming X-ray beam. The detector scan was varied from 10° to 67° at a scan rate of 0.5 s step^{-1}.

2.2.2. Atomic Force Microscopy (AFM)

Surface morphology of the Mo films was also studied employing atomic force microscopy (AFM). Samples were mounted on sapphire substrates using double sided tape and AFM experiments were performed (Ntegra, NT-MDT, UK) in contact mode. AFM images were acquired using probes with a 0.01–0.5 N m^{-1} Force constant (NT-MDT CSG/10). Several measurements were made, prior to actual surface imaging analysis of Mo films, to assure the probe tip quality. Specifically, tip quality was qualitatively assessed by examining the images for clarity and presence of artifacts. The standards provided by the instrument manufacturer were employed for calibration. The most commonly measured roughness, that is, the average surface roughness (R_a), parameter of the nc-Mo films was calculated using.[33]

$$R_a = \frac{1}{L}\int_0^L |Z(x)|dx \tag{2}$$

where $Z(x)$ is the function that describes the surface profile analyzed interms of height (Z) and position (x) of the sample over the evaluation length "L".

The other roughness parameters are Root mean square roughness (R_q), ten point average roughness (R_Z) third highest peak to third lowest valley height (R_{3Zi}). Surface roughness refers to variations in height and is measured either along a single line profile or along a set of parallel line profiles. R_a is the arithmetic average of the absolute values of the surface height deviations measured from the mean plane. In this analysis, each image of 500×500 nm^2 has 65 536 sampling points. R_q is the standard deviation of the variance from the mean plane of these sampling points. Surface skewness (RSK) characterizes the symmetry of distribution. Skewness and kurtosis parameter are important in giving better understanding of the surface. These single numerical parameters, R_a and R_q, are useful mainly for classifying surfaces of the same type that are produced by the same method.

2.2.3. Nano-Mechanical Properties (Hardness and Elastic Modulus)

The deposited Mo films were analyzed to determine their mechanical properties; hardness (H) and reduced elastic modulus (E_r) were obtained by nanoindentation tests (Hysitron T1750 Tribo nanoindentor). The nanoindentation measurements were made employing a triangular pyramid Berkovich diamond indenter with a normal angle of 65.3° between the tip axis, and the faces of the triangular pyramid and the effective size of the apex are about 100 nm. The system automatically perform seven indents in the shape of an "H" (three on each side for the legs and one in the middle). This is the simplest pattern to find and it is recommended to use this during most probe (indenter tip) calibrations. The "H" pattern will perform on fused quartz and during this the indents are spaced 15 μm apart for low load systems. The load versus displacement curves and indentation patterns are correlated with the original probe calibration sheet,

that is, supplied with each probe. The method developed by Oliver and Pharr[34] was employed to calculate the mechanical characteristics (H and E_r) with the help of loading and unloading curves. From the slope of the unloading curve, the elastic modulus (E_r) can be calculated by finding the stiffness (S) of the film using the relation:

$$E_r = \frac{\sqrt{\pi}}{2}\frac{S}{\sqrt{A}} \tag{3}$$

where A is defined as the area of contact at peak load. To find the hardness, the same value for the area of contact is used along with the maximum load (P_{max}) in:

$$H = \frac{P_{max}}{A} \tag{4}$$

The load-controlled indentation tests were performed initially on each sample to determine the maximum depth that would not be more than 10% of the total film thickness. This procedure is adopted not only to avoid the substrate effects, but also to obtain the reliable mechanical properties of Mo films. Also, in order to account for the statistical data and reliability, seventeen indents of selected 250 μN load were performed at 0.2 s^{-1} strain rate, and the average H and E_r values were calculated on each sample. The final average H and E_r values were considered to further assess the materials' mechanical behavior.

2.2.4. Scratch Testing

For nanostructured samples, film, or coating, the adhesion to the substrate is one of the paramount characteristics related the coating quality and life endurance. Therefore, the Mo film adhesion was analyzed by nano-scratch test (Hysitron T1750 Tribo nanoindentor). This test was performed at room temperature under the load increments from 0 to 8000 μN. The same standard triangular pyramid Berkovich diamond indenter tip has been used. The length of the scratch was 16 μm, and the scratch speed was 0.18 μm s^{-1}.

3. Results

3.1. Crystal Structure

Figure 2 shows the GIXRD patterns of Mo films deposited under variable P_{Ar}. It can be noted that the Mo films exhibit a marked difference in diffraction patterns (Figure 2a) with increasing P_{Ar}. Observation of (110) peak at 40.5° clearly indicates that the Mo films exhibit (110) preferential growth.[19,21] Moreover, there is a considerable decline in the peak intensity with increasing P_{Ar} from 3 to 25 mTorr. This behavior is attributed to the deterioration of the crystalline quality with increasing P_{Ar}. The Mo films deposited at the lowest P_{Ar} (3 mTorr) exhibit dominance in the (110) peak intensity. In order to better understand peak intensity variation and to derive quantitative information, high resolution scans were performed on the (110) reflection. Figure 2b shows the high-resolution scans of the (110) peak as a function of P_{Ar}. The data clearly indicates the peak broadening along with a small peak shift with increasing P_{Ar}. Considerable peak broadening noted at the highest P_{Ar} (25 Torr) indicates degradation of crystallinity at higher pressures. Thus, XRD results confirm a clear dependence of crystallinity of Mo films on P_{Ar}. Interdependency between texture development and processing parameters in physical vapor deposited thin films can be, in general, explained based on thermodynamics or growth kinetics.[35] Therefore, effect of P_{Ar} on the crystal structure and growth behavior of Mo films can be attributed to the difference in adatom mobility, which influences the texture and/or preferred orientation of the films grown.[23]

Using XRD data, the lattice parameter values were determined. The "a" values of all the Mo films were found to be 3.16 (±0.01) Å. The average crystallite size "d" was calculated using the Scherrer's equation[16,36]:

$$d = \frac{0.9\lambda}{\beta \cos\theta} \tag{5}$$

where d is the average crystallite size, λ is the wavelength of X-rays, β is the width of the peak at its half intensity, and θ is the angle of the peak.

The functional P_{Ar}-d dependence in Mo films is shown in **Figure 3**. The maximum value of d is found to be 18 (±1) nm for $P_{Ar} = 3$ mTorr. With the increase in P_{Ar}, the size gradually decreases to 7 (±2) nm for a P_{Ar} of 19 mTorr. As noted in a PVD films, the P_{Ar}-d relationship can be decimated to the mean free path[23] and surface damage.[24] At lower P_{Ar}, the mean free path increases which results in a decrease in collisions between the substrate and the target. This leads to an increase in net kinetic energy of the sputtered species giving a higher mobility of particles on the film surface. A resulting higher driving force is experienced by the sputtered species which is driven to a preferred lattice site, consequently leading to nucleation and growth.[23,24] Hence, the increase in film crystallinity can be attributed to this mechanism arising due to the higher d values at lower P_{Ar}. Higher P_{Ar} must be leading to surface damage leading to a deteriorated crystal structure.

3.2. Microstructure and Morphology

The morphology, average surface roughness (R_a), root mean square roughness (R_q), and the grain size were analyzed using AFM in Contact Mode (CM). Quantitative analysis was performed in CM instead of tapping mode to reduce any deviation from feedback. Images of the Mo film morphology are shown in **Figure 4**a, where the effect of P_{Ar} on the morphology evolution can immediately be observed. Grain analysis (Figure 4b) performed on the surface area revealed the Mo film produced at the lowest P_{Ar} exhibit dense areas with small porous features. The frequency of gas-phase collisions is reduced when the P_{Ar} is low and this in turn increases the kinetic energy of the sputtered Mo atoms leading to the dense morphology of the Mo film with less intra-grain voids porous grains. This observation is in agreement with reports exist in the literature.[17,21] As P_{Ar} increases, the film surface becomes smoother and grain sizes enlarge gradually while intra-grain

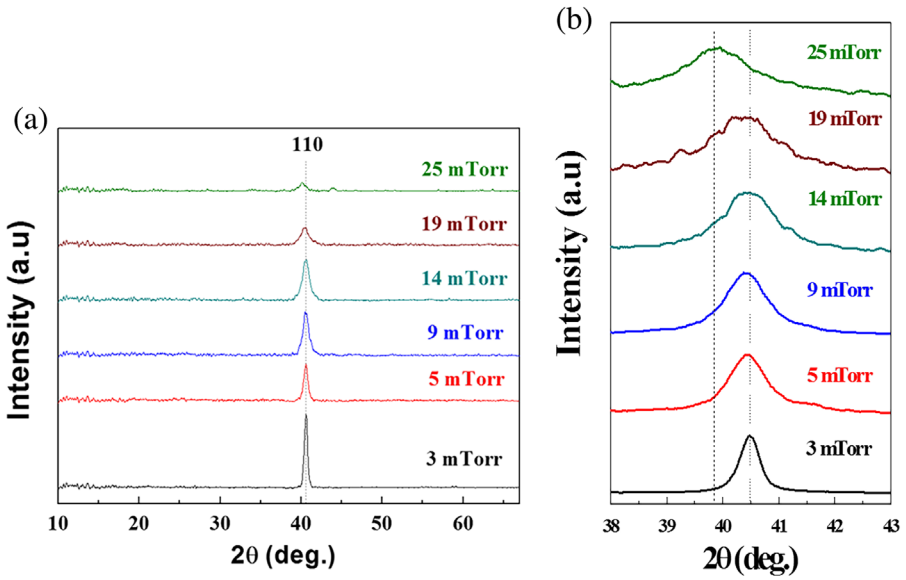

Figure 2. a) GIXRD patterns of Mo films deposited under variable P_{Ar}. b) High resolution scan of Mo (110) peak.

voids become less and less visible (Figure 4c). This correlates well with R_a and R_q as we see a decrease in surface area roughness with an increase in deposition pressure (Figure 4d).

3.3. Mechanical Properties

3.3.1. Indentation Load (L) – Penetration Depth (d_h) Characteristics

The data of peak indentation load (L) - indentation depth (d_h) of the nc-Mo films are shown in **Figure 5**. While nano-indentation measurements provides a simple and quick method for obtaining information about the mechanical properties of thin films, the L-d_h characteristics must be considered for reliable mechanical property determination.[37,38] The L-d_h data (Figure 5) indicate that all the Mo films exhibit the similar response, that is, an increase in the d_h with respect to increasing L, which was varied from 100 to 2000 μN. At the initial load, that is, at 100 μN, the depth was ≈8–9 nm for Mo films deposited at $P_{Ar} = 3$ mTorr. However, at 250 μN, the film depth reaches ≈11–12 nm, which is about 10% of the film total thickness. It can be noted that, at 250 μN, d_h value increases to 20 nm with increasing P_{Ar} from 3 to 25 mTorr. Whereas, at $L = 2000$ μN, d_h increases to 80–90 nm range for Mo films deposited at higher $P_{Ar} = 19$–25 mTorr. The relatively high values of d_h and the observed differences are due to the microstructure of the nc-Mo films.

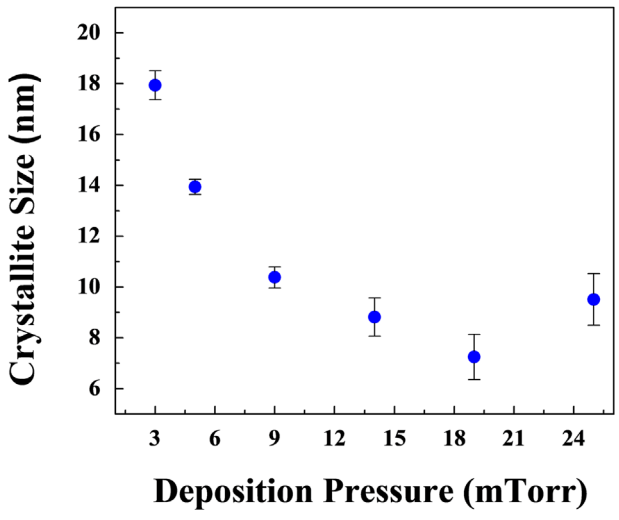

Figure 3. The variation of average crystallite size with P_{Ar}.

3.3.2. Hardness (H) and Elastic Modulus (E_r)

The experiments to determine H and E_r were performed at a critical load of 250 μN, where the penetration depth was ≈10% of the total film thickness which is acceptable to avoid the substrate effects.[39] The variation of H and E_r values with P_{Ar} is shown in **Figure 6**. To better compare the data and to indicate the correlation, the average crystallite size is indicated on the top-linked X-axis. It is evident that P_{Ar} significantly affects the mechanical properties of nc-Mo films. As shown in Figure 6, the H and E_r decreases with increasing P_{Ar}. The high values of H and E_r are 25 and 355 GPa, respectively, are noted for Mo films deposited at $P_{Ar} = 3$ mTorr. The microstructure of the Mo films predominantly contributes to the enhanced H and E_r values.

3.3.3. H/E_r and H^3/E_r^2

The ratio parameters, namely H/E_r and H^3/E_r^2 were calculated to further assess the effect of P_{Ar} on mechanical behavior of Mo films. H/E_r and H^3/E_r^2 along with H and E_r have played a significant role to gain insights about the mechanical

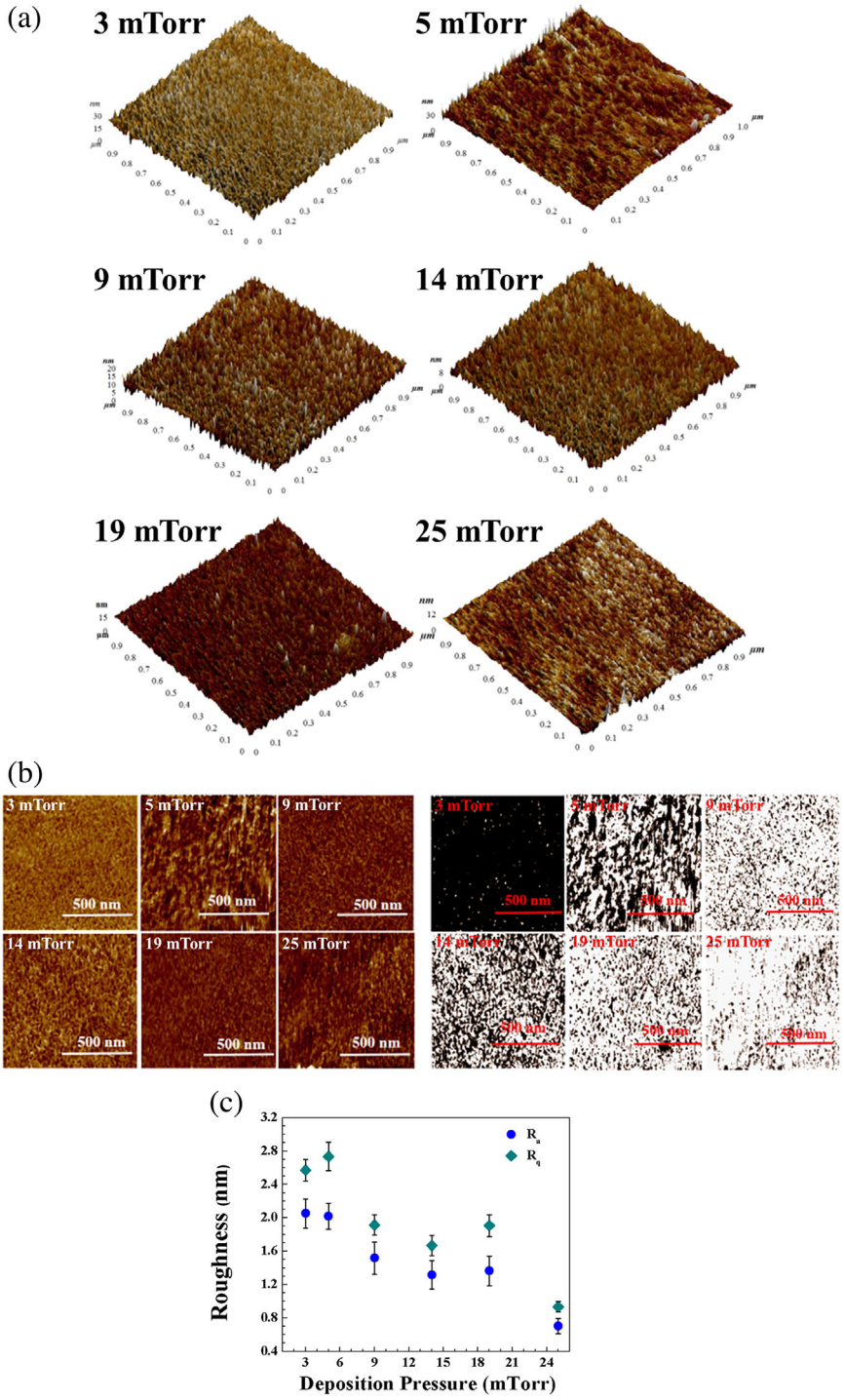

Figure 4. a) AFM micrographs for Mo films deposited at different pressure conditions. b) AFM micrographs for Mo films deposited at different pressure conditions. c) Grain analysis for Mo films deposited at different pressure conditions. d) Correlation between deposition pressure and roughness of Mo films.

performance of thin films and coatings.[37,39,40] An extension of this principle can be seen in **Figure 7**, which shows a strikingly similar functional P_{Ar} dependence for both H/E_r and H^3/E_r^2.

The ratio between H and E_r is referred to as plasticity index[41] (sometimes it is also indicated as coating durability),[42] which is an indicative of the limit of elastic behavior of the films. Similarly, H^3/E_r^2 is a reliable indication of a coating's resistance to plastic deformation and referred to as toughness.[43] Thus, H/E_r and H^3/E_r^2 are excellent measures to estimate films' cracking resistance and in further evaluation of its wear performance. The H/E_r ratio decreases with increasing P_{Ar}. The values varied from 0.070 to 0.055 for variation in P_{Ar}

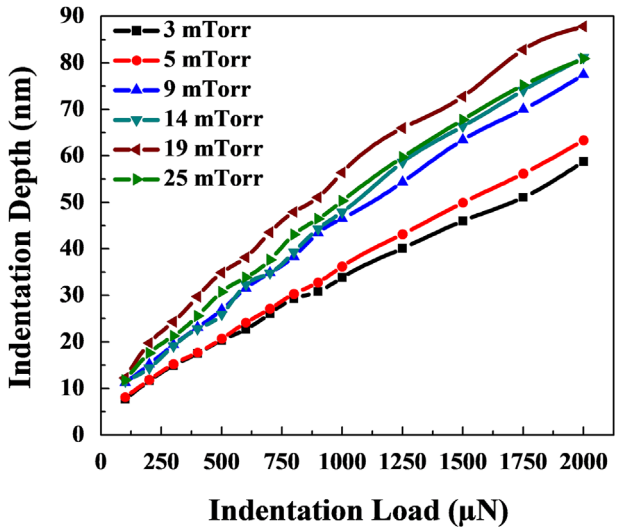

Figure 5. The indentation load–penetration depth characteristics of Mo films.

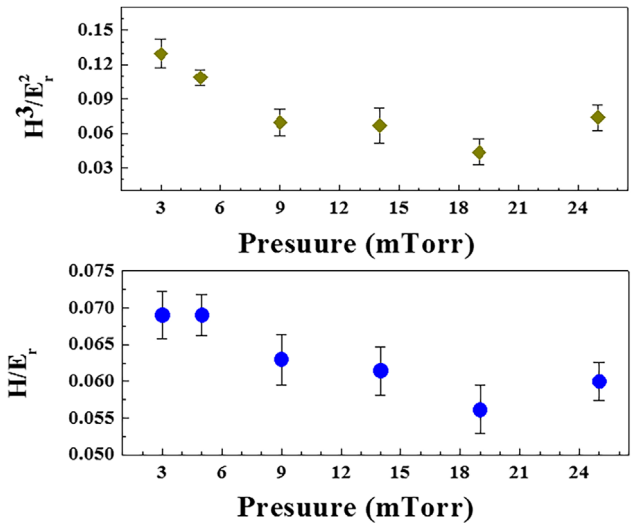

Figure 7. The effect of P_{Ar} on a) H/E_r and b) H^3/E_r^2 values.

from 3 to 25 mTorr. The H^3/E_r^2values started at 0.13 for 3 mTorr and then decreased to 0.05 for 19 mTorr.

3.4. Adhesion and Interfacial Bonding – Scratch Testing

The scratch test results of nc-Mo films are shown in **Figure 8**. It can be observed that as the load increases, the corresponding depth and width of the scratch follows suite. Cohesive failure is observed when area surrounding the scratch undergoes deformation but leaving the remainder of film unscathed.[44] An adhesive or interfacial failure is attributed to the incision of film along the direction of scratch which further leads to a complete detachment[45] or catastrophic failure.[46] It is pertinent to note that the films in context are not susceptible to delamination and end up with pile up deformation resulting from the load application, as shown in Figure 8b. The depth profiles show the cross-section of the Mo films at the maximum applied force along the scratch. An indication of positive depth means the indenter is moved below the initial surface while negative scratch depth indicates that the indenter is located above the initial sample surface. Evidently, the depth profile cross-sections obtained at the maximum 8000 μN force exhibits that at lower P_{Ar} the indenter penetrates less when compared to those Mo films deposited at higher P_{Ar}. This behavior matches well with hardness (Figure 6). Also, no channel cracking/delamination of the Mo films is noted in these nano-scratch tests.

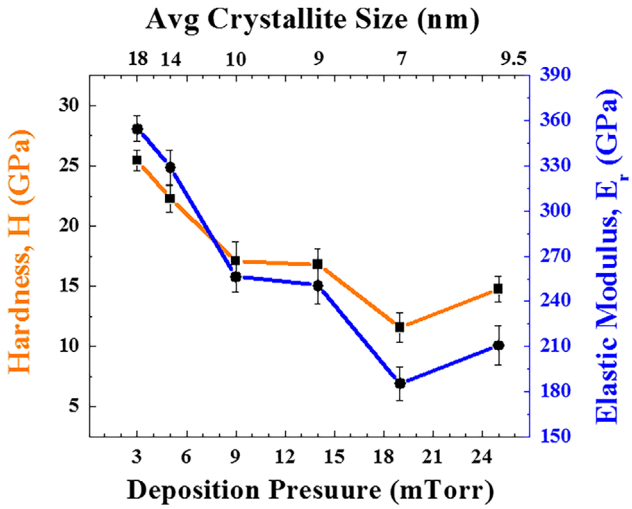

Figure 6. The variation of H and E_r of Mo films with P_{Ar}. The functional dependence of H and E_r values on the crystallite size can also be noted from the top-linked X-axis.

4. Discussion

The XRD, AFM, nano-indentation, and nano-scratch testing results can be conveniently gathered together to understand the crystal structure, morphology evolution, and mechanical properties of Mo films as a function of P_{Ar}. As evident from results, P_{Ar} strongly influences the microstructure and mechanical properties of Mo films. Note that the temperature and pressure during deposition influences the crystal growth and structure, grain size and morphology.[47,48] The influence of P_{Ar} on crystal structure and (110) orientation of Mo films can thus be ascribed to the entwining effect arising from thermodynamic and kinetic factors. The P_{Ar} also dictates the adatom mobility and ultimately influences the film texturing.[23,47] The mean free path (λ_m) of sputtered species which is dependent on P_{Ar} influences the deposition rate and growth behavior of films.[49] The relation between mean free path and pressure is governed by[49]:

$$\lambda_m = \frac{k_B T}{\sqrt{2}(r_g + r_m)^2 P} \tag{6}$$

where k_B is the Boltzmann constant, T is the absolute temperature, P is the pressure, and r_g and r_m are the ionic radii of Ar gas and Mo metal, respectively. An increase in P_{Ar}

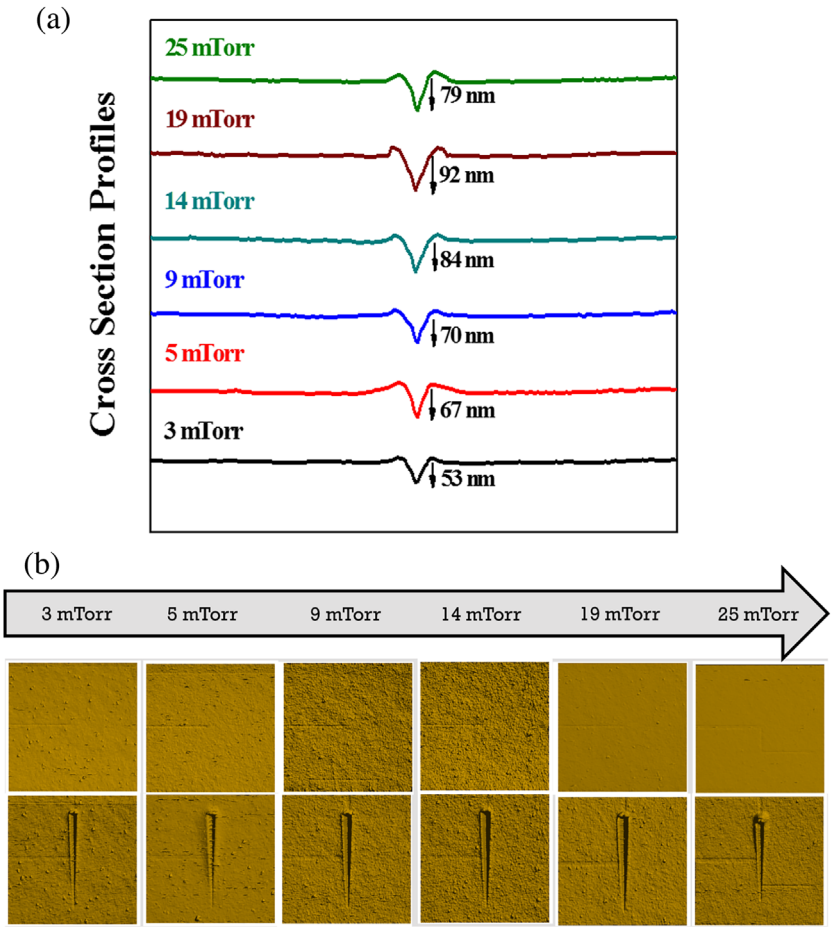

Figure 8. a) The depth profiles of Mo films with variable P_{Ar}. b) Pre and Post-scratch images of Mo films.

pressure increases ionization resulting in considerable amount of Ar^+ ions to interact with target and subsequently increases the sputter rate. The formation of crystalline Mo films can be attributed to the optimum T_s. In general, the crystalline versus amorphous structure of a metal film resulting from PVD is influenced by T_s.[50] It may further be noted, since no substrate bias is employed, the thermal energy is partaken from $T_s = 200\,^{\circ}C$, which is optimum for the said purpose. The resulting Mo films are nanocrystalline in nature, but they deteriorate at higher P_{Ar}. This characteristic growth behavior is important to consider since the Mo films for application in solar cells require fabrication of component layers in the device at elevated temperatures.[16,19,22,28–31]

The (110) preferential growth of nc-Mo films can be explained based on the minimum energy considerations.[51] The preferential growth of metal films is primarily influenced by surface diffusion, which is dependent on the deposition conditions. Under sufficient mobility of ad-atoms, the lowest-surface energy plane becomes the preferred orientation. Therefore, the observed (110) preferential growth of Mo films as noted in XRD data is due to the minimization of energy.[23] Therefore, under given conditions of T and P, which are optimum to promote the formation of crystalline films, the growth of *bcc* Mo with (110) preferential growth is thermodynamically preferred. Such a preferred (110) growth has been reported for sputter-deposited *bcc* Mo[52] and *bcc* W-Mo films.[23,48]

The effect of P_{Ar} is demonstrated by the AFM data, which indicates an evolution from a dense fine-fiber to an intra-grain void structure. We hypothesize that the change in microstructure is a result of the varying particle energy with P_{Ar}. The strong dependence of microstructure on the particle energy is generally observed in sputter-deposited films. Contrarily, a hint of porosity in tandem with a well maintained dense structure at an intermediate P_{Ar} may be a significant indicator of reduced adatom energy which further implies a decrease in surface mobility.[47] This lower particle energy, leading to a limited diffusion explains the microstructure of Mo films at higher P_{Ar}. Similar behavior was observed in a wide variety of metals and alloys namely W, Ti, Cr metals, and W–B alloys.[47]

To understand the substantial improvement in the mechanical properties, an understanding of microstructure variation with P_{Ar} is reasonable. As mentioned earlier, the films deposited at $P_{Ar} = 3$ mTorr exhibit best hardness and elastic modulus. The H and E_r represent the intrinsic material properties, which are governed by strength of the chemical bonds of the constituent atoms in the materials. A substantial role is played by size reduction which helps improving the mechanical characteristics of the Mo films. Reduction in grain size hinders the propagation

of dislocations through the grain boundaries.[5,53] This results in an elevated stress concentration at the grain boundaries owing to dislocation pile-up. Hall–Petch relationship can be employed to decrypt this phenomenon, as it postulates, hardness to be inversely proportional to the square root of size.[54] It has already been established that the intragranular nanotwins supports material strength. Twin boundaries act as an analogous high-angle grain boundary and disrupts the propagation of dislocations. It has been specifically found to be highly efficient in disrupting single dislocations' propagation. In analogy with Hall–Petch relationship, hardness can also be related to the grain size by[55]:

$$H_\gamma = H_0 + k_H d^{-1/2} \tag{7}$$

where H_0 and k_H are constants. Hardness essentially means the resistance of a material to plastic deformation under an applied load. It may duly be noted that phenomenon like relaxation at grain boundaries, fine grain size may result in a decreased strength and hence a reverse Hall–Petch effect.[56] Hence, with a fair degree of certainty, crystallite size reduction along with dense microstructure can be attributed to the established values of H and E_r.

5. Conclusions

Molybdenum nc-films were deposited with varying sputtering pressure of argon in the range of 3–25 mTorr. Structural, surface imaging, and mechanical characterization of the deposited Mo films using a wide variety of analytical methods elucidate the effect of P_{Ar} on the crystal structure, microstructure, and mechanical properties of *nc*-Mo films. Evident from the structural studies, Mo films crystallize in *bcc* structure and exhibit preferred (110) growth. However, higher P_{Ar} deteriorates the crystal quality due to difference in the mobilities of sputtered species. The d-P_{Ar} relationship established suggests that Mo films with a crystallite size controlled in the range of 5–19 nm can be realized by carefully controlling P_{Ar}. Based on the combined XRD, SEM, AFM and nano-indentation data analyses, the "*size reduction and microstructure*" effect is remarkable on the mechanical properties of Mo films. The hardness and modulus of elasticity of the *nc*-Mo films deposited at lower P_{Ar} were higher but decreases continuously with increasing P_{Ar}. The best mechanical properties, $H = 25$ GPa, $E_r = 360$ GPa, $H/E_r = 0.07$, and $H^3/E_r^2 = 0.13$, were achieved in Mo films deposited under optimum deposition conditions. The microstructure-mechanical property correlation established in this work may be useful to provide a road-map to produce nanocrystalline Mo films for optical and electronic device applications.

Acknowledgement

The authors acknowledge, with pleasure, support from the National Science Foundation (NSF) with the NSF-PREM grant #DMR-1827745.

Conflict of Interest

The authors declare no conflict of interest.

Keywords

microstructure, molybdenum, nanocrystal, nano-mechanical properties

Received: May 7, 2018
Revised: June 19, 2018
Published online: September 18, 2018

[1] L. Huang, J. Lu, M. Troyon, *Surf. Coat. Technol*. **2006**, *201*, 208.
[2] M. B. Lowry, D. Kiener, M. M. LeBlanc, C. Chisholm, J. N. Florando, J. W. Morris, A. M. Minor, *Acta Mater*. **2010**, *58*, 5160.
[3] T. C. Chou, T. G. Nieh, S. D. McAdams, G. M. Pharr, W. C. Oliver, *J. Mater. Res*. **2011**, *7*, 2774.
[4] W. D. Nix, *Miner. Met. Mater. Soc*. **1988**, *20A*, 2217.
[5] S. Kobayashi, S. Tsurekawa, T. Watanabe, *Acta Mater*. **2005**, *53*, 1051.
[6] S. C. Tjong, H. Chen, *Mater. Sci. Eng. R* **2004**, *45*, 1.
[7] M. A. Meyers, A. Mishra, D. J. Benson, *Prog. Mater. Sci*. **2006**, *51*, 427.
[8] S. L. Frederiksen, K. W. Jacobsen, J. Schiøtz, *Acta Mater*. **2004**, *52*, 5019.
[9] T. Eliash, M. Kazakevich, V. N. Semenov, E. Rabkin, *Acta Mater*. **2008**, *56*, 5640.
[10] E. Hall, *Proc. Phys. Soc. B* **1951**, *64*, 747.
[11] N. J. Petch, *J. Iron Steel Inst*. **1953**, *174*, 25.
[12] Y. Tang, E. M. Bringa, M. A. Meyers, *Sci. Eng. A* **2013**, *580*, 414.
[13] C. Schuh, T. Nieh, T. Yamasaki, *Scr. Mater*. **2002**, *46*, 735.
[14] S.-Y. Chang, T.-K. Chang, *J. Appl. Phys*. **2007**, *101*, 033507.
[15] C. Schuh, T. Nieh, H. Iwasaki, *Acta Mater*. **2003**, *51*, 431.
[16] J.-H. Cha, K. Ashok, N. J. S. Kissinger, Y.-H. Ra, J.-K. Sim, J.-S. Kim, C.-R. Lee, *J. Korean Phys. Soc*. **2011**, *59*, 2280.
[17] J. H. Scofield, A. Duda, D. Albin, B. Ballard, P. Predecki, *Thin Solid Films* **1995**, *260*, 26.
[18] J. Bartolome, M. Dıaz, J. Requena, J. Moya, A. Tomsia, *Acta Mater*. **1999**, *47*, 3891.
[19] Z.-H. Li, E.-S. Cho, S. J. Kwon, *Appl. Surf. Sci*. **2011**, *257*, 9682.
[20] T. Wada, N. Kohara, S. Nishiwaki, T. Negami, *Thin Solid Films* **2001**, *387*, 118.
[21] G. Zoppi, N. S. Beattie, J. D. Major, R. W. Miles, I. Forbes, *J. Mater. Sci*. **2011**, *46*, 4913.
[22] R. Tran, Z. Xu, N. Zhou, B. Radhakrishnan, J. Luo, S. P. Ong, *Acta Mater*. **2016**, *117*, 91.
[23] G. Martinez, C. V. Ramana, *AIP Adv*. **2017**, *7*, 125201.
[24] K. S. Harsha, *Principles of Vapor Deposition of Thin Films*, Elsevier, Oxford, UK **2005**.
[25] K. Miyoshi, *Solid Lubrication Fundamentals and Applications*, CRC Press, New York, USA **2001**.
[26] W. Dresel, *Lubricants and Lubrication*, John Wiley & Sons, Seiten, Germany **2007**.
[27] C. Donnet, A. Erdemir, *Tribol. Lett*. **2004**, *17*, 389.
[28] J.-H. Yoon, S. Cho, W. M. Kim, J.-K. Park, Y.-J. Baik, T. S. Lee, T.-Y. Seong, J.-H. Jeong, *Sol. Energy Mater. Sol. Cells* **2011**, *95*, 2959.
[29] S. Wang, C. Hsu, F. Shiou, P. Huang, D. Wen, *J. Electron. Mater*. **2013**, *42*, 71.
[30] M. Jubault, L. Ribeaucourt, E. Chassaing, G. Renou, D. Lincot, F. Donsanti, *Sol. Energy Mater. Sol. Cells* **2011**, *95*, S26.
[31] X. Dai, A. Zhou, L. Feng, Y. Wang, J. Xu, J. Li, *Thin Solid Films* **2014**, *567*, 64.
[32] R. Zhang, Z. Huo, X. Jiao, B. Du, H. Zhong, Y. Shi, *J. Nanosci. Nanotechnol*. **2016**, *16*, 8154.
[33] R. De Oliveira, D. Albuquerque, T. Cruz, F. Yamaji, F. Leite, in "*Atomic Force Microscopy*" ed. by V. Bellito, InTech Open Book Series, **2012**.
[34] W. C. Oliver, G. M. Pharr, *J. Mater. Res*. **1992**, *7*, 1564.
[35] U. Oh, J. H. Je, *J. Appl. Phys*. **1993**, *74*, 1692.
[36] B. Cullity, *Elements of X-ray diffraction*, Addison-Wesley Publishing Co., Inc., USA **1956**, p. 78.

[37] A. Leyland, A. Matthews, *Wear* **2000**, *246*, 1.
[38] A. Rosenkranz, L. Reinert, C. Gachot, H. Aboufadl, S. Grandthyll, K. Jacobs, F. Müller, F. Mücklich, *Adv. Eng. Mater.* **2015**, *17*, 1234.
[39] L. Zhou, Y. Yao, *Mater. Sci. Eng. A* **2007**, *460–461*, 95.
[40] B. Jönsson, S. Hogmark, *Thin Solid Films* **1984**, *114*, 257.
[41] A. Leyland, A. Matthews, *Surf. Coat. Technol.* **2004**, *177–178*, 317.
[42] Y. Huang, F. Zhang, K. Hwang, W. Nix, G. Pharr, G. Feng, *J. Mech. Phys. Solids* **2006**, *54*, 1668.
[43] D. Sherman, D. Brandon, *Adv. Eng. Mater.* **1999**, *1*, 161.
[44] F. Ashrafizadeh, *Surf. Coat. Technol.* **2000**, *130*, 186.
[45] H. Sojoudi, M. R. Walsh, K. K. Gleason, G. H. McKinley, *Adv. Mater. Interfaces* **2015**, *2*, 1500003.
[46] P. M. Johnson, C. M. Stafford, *ACS Appl. Mater. Interfaces* **2010**, *2*, 2108.
[47] F. Vüllers, R. Spolenak, *Thin Solid Films* **2015**, *577*, 26.
[48] G. Martinez, C. V. Ramana, *Adv. Eng. Mater.* **2017**, *19*, 1700354.
[49] J. A. Thornton, *J. Vac. Sci. Technol.* **1974**, *11*, 666.
[50] E. J. Rubio, T. E. Mates, S. Manandhar, M. Nandasiri, V. Shutthanandan, C. V. Ramana, *J. Phys. Chem. C* **2016**, *120*, 26720.
[51] I. Petrov, F. Adibi, J. Greene, W. Sproul, W. D. Münz, *J. Vac. Sci. Technol. A* **1992**, *10*, 3283.
[52] Y. Shen, *Mater. Sci. Eng. A* **2003**, *359*, 158.
[53] Y. D. Kolekar, L. Sanchez, E. J. Rubio, C. V. Ramana, *Solid State Commun.* **2014**, *184*, 34.
[54] R. Armstrong, *Metall. Mater. Trans. B* **1970**, *1*, 1169.
[55] a) N. Hansen, *Scr. Mater.* **2004**, *51*, 801; b) T. Nieh, J. Wadsworth, *Scr. Metall. Mater.* **1991**, *25*, 955.
[56] C. Carlton, P. Ferreira, *Acta Mater.* **2007**, *55*, 3749.

